*Optica Applicata, Vol. XLIII, No. 4, 2013*
DOI: 10.5277/oa130421

# Spectral analysis of dynamic laser speckle patterns by using a full-field temporal modulation method

DAKE WANG*, EMILY CHASTEEN, CHISOM ONYEUKU

Department of Physics, Furman University, Greenville, South Carolina 29613, USA

* Corresponding author: dake.wang@furman.edu

We introduce an approach for analyzing the power spectrum of the time-varying intensity in the dynamic laser speckle patterns. The method is free from the limitation imposed by the Nyquist criterion on the minimum sampling rate. The temporal modulation shifts the intensity fluctuation spectrum by an amount that is equal to the modulation frequency. The subsequent integration of the intensity signal, performed at each detector pixel, acts effectively as a low-pass filter allowing the extraction of the spectral component at the modulation frequency. Within the speed range from 1 to 10 mm/s investigated in our experiment, the result demonstrates that the moving speed of the diffuse object can be determined with a good accuracy.

Keywords: laser speckle, spectral analysis, light scattering.

## 1. Introduction

The interference of coherent light reflected by or transmitted through diffuse objects gives rise to the random speckle patterns. If the scattering objects are also in motion, the speckle patterns will vary with time, creating translating/rotating and boiling dynamic speckle patterns. By analyzing the temporal fluctuation of the intensity, the motion of the objects can be revealed. Laser speckle contrast analysis (LSCA) techniques such as laser speckle spatial and temporal contrast analysis have been developed for the full-field monitoring of dynamics in diffuse media [1–6]. These LSCA techniques offer the full-field imaging capability with excellent spatial and temporal resolutions. However, because of the complexity of the scattering process in diffuse media and the nature of the dynamic speckles, it is still difficult to apply LSCA techniques as quantitative tools for the interpretation of the complex dynamic processes presented in inhomogeneous strongly-scattering objects [7, 8].

The intensity fluctuating spectra of the scattering light can be obtained by using photon correlation spectroscopy and laser Doppler techniques. Although they suffer from similar problems, such as the multiple-scattering effect, as do LSCA techniques [8–12], an intensity fluctuating spectrum is substantially more informative than

just a single speckle contrast reading obtained with LSCA techniques. The information regarding the scatterers and their dynamics can be either inferred from the spectral features such as the cutoff frequencies and the shift of spectral bands [13, 14], or determined from the zero-order and first-order moments of the spectra [15, 16]. This advantage in the quantitative analysis is one of the reasons for the widespread application of photon correlation spectroscopy and laser Doppler techniques for perfusion and flow measurements [11–24].

In both photon correlation spectroscopy and laser Doppler technique, the time--varying intensity must be recorded at a sampling rate that is at least two times that of the signal bandwidth in order to truthfully recover the autocorrelation function and the frequency spectrum. This requirement on the minimum sampling rate is easily met by the use of single-channel detectors or streak cameras. However, in many biomedical and micro-fluidic applications where the spatial distributions of velocity or flow rate are to be imaged, the use of single-channel detector or streak cameras would require the scanning of the objects, meaning that the dynamical events occurring at two different spots on the object may not be recorded simultaneously. Full-field methods demand the use of multi-channel detectors such as a charge-coupled device (CCD) which often have limited frame-rates when operating at full resolution. The state-of-art complementary metal-oxide semiconductor (CMOS) detectors are capable of operating at frame rates up to a few kHz and more, albeit at reduced resolutions and regions of interest (ROI) [25, 26]. To overcome the limitation imposed by the speed of the multi--channel detectors, molecular filters have been used to construct a full-field Doppler velocimetry [27]. However, this technique is effective for Doppler shifts in the MHz range which limits its use to applications where very high flow speeds are involved.

In this work, we introduce a full-field method based on the temporal modulation of the light intensity and the subsequent low-pass filtering implemented via the signal integration. Because this method does not rely on the use of fast frame rates and high-speed recordings, it can be readily implemented with currently available multi--channel detectors. As the modulation frequency can be chosen over a wide range, it has the potential for probing a wide range of Doppler shifts. This large dynamic range makes it possible for imaging the speed and flow distributions in the presence of large speed variations. The aim of this work is to elucidate on the basic concepts involved in this method, and to demonstrate its feasibility for investigating the power spectrum of the time-varying intensity from a moving random phase object.

## 2. Theoretical development

The spectral analysis procedure often involves sending the intensity signal $I(t)$ into a band-pass filter whose bandwidth is very small. The output of the filtering can be regarded as the spectral component of the input signal at the central frequency of the filter. In order to construct the full spectrum of $I(t)$, the central frequency of the filter needs to be scanned over a frequency range.

Instead of shifting the band-pass filter, we shifted the spectrum of the signal itself by the sinusoidally modulating the light intensity. The original intensity signal $I(t)$ becomes the modulated intensity signal: $I(t, f_0, \varphi) = [1 + M\cos(2\pi f_0 t + \varphi)]I(t)$, where $M$ is the modulation depth which is smaller than unity, $f_0$ is the modulation frequency, and $\varphi$ is the phase angle. In the frequency domain, the modulation gives rise to two side bands which are located at $-f_0$ and $f_0$. The Fourier transform of the modulated intensity is given by the convolution theorem as:

$$X(f, f_0, \varphi) = \left\{\delta(f) + \frac{1}{2}M\left[e^{-i\varphi}\delta(f + f_0) + e^{i\varphi}\delta(f - f_0)\right]\right\} \otimes X(f) = \\ = X(f) + \frac{1}{2}M\left[e^{-i\varphi}X(f + f_0) + e^{i\varphi}X(f - f_0)\right] \tag{1}$$

If the modulated intensity signal is then sent into a low-pass filter with infinitely narrow bandwidth such as a Dirac $\delta$ function, we get, in the frequency domain:

$$\delta(f)X(f, f_0, \varphi) = \delta(f)\left\{X(0) + M\left[\cos(\varphi)X_R(f_0) + \cos(\varphi)X_I(f_0)\right]\right\} \tag{2}$$

where $X_R(f_0)$ and $X_I(f_0)$ are the real and imaginary part of the spectrum at the modulation frequency, respectively. Therefore, the frequency-domain output $F(f_0, \varphi)$ is:

$$F(f_0, \varphi) = X(0) + M\left[\cos(\varphi)X_R(f_0) + \cos(\varphi)X_I(f_0)\right] \tag{3}$$

To obtain the power spectrum, the phase angle is changed by 90° from $\varphi$, and the frequency-domain output, after the filtering, changes from $F(f_0, \varphi)$ to $F(f_0, \varphi + \pi/2)$, accordingly. It follows in a straightforward manner that the power spectrum at the modulation frequency can be determined as:

$$S(f_0) = \frac{1}{M^2}\left[F(f_0, \varphi) - X(0)\right]^2 + \frac{1}{M^2}\left[F\left(f_0, \varphi + \frac{\pi}{2}\right) - X(0)\right]^2 \tag{4}$$

In this work, the low-pass filtering is implemented via the signal integration. What is actually recorded at the detector is not the instantaneous value of $I(t)$, but its integrated value within a limited integration time of $\tau$ [28]:

$$\tilde{I}(t) = \int_t^{t+\tau} I(t')\mathrm{d}t' = \int_{-\infty}^{+\infty} \mathrm{rect}(t - t')I(t')\mathrm{d}t' \tag{5}$$

The integrated intensity $\tilde{I}(t)$ can be regarded as the convolution between a rectangular function and $I(t)$. Thus, its Fourier transform $\tilde{X}(f)$ is the multiplication of the spectrum $X(f)$ and a sinc-like function:

$$\tilde{X}(f) = \tau \sin[c(\tau f)]X(f) \tag{6}$$

In the limit of very long integration time, the sinc-like function approaches the Dirac $\delta$ function, and Eq. (6) approaches Eq. (2). In practice, the integration time needs to be much longer than the decorrelation time associated with the time-varying intensity signal.

By replacing the sinc-like function with the $\delta$ function in Eq. (6), the DC component $X(0)$ is obtained. Likewise, $F(f_0, \varphi)$, and $F(f_0, \varphi + \pi/2)$ are determined from Eq. (6), in the presence of the intensity modulation. The three quantities are then substituted into Eq. (4) to calculate the power spectrum at the modulation frequency $f_0$.

## 3. Experimental measurement

In this work, the modulation needs to be performed with two different phase angles. To ensure that the two intensity signals: $I(t, f_0, \varphi)$ and $I(t, f_0, \varphi + 90°)$ differ only in their phase angles, their modulation and the subsequent recording must be performed simultaneously while the diffuse object is being moved. Figure 1 shows the schematics of the optical system consisting two optical paths each of which processes one intensity signal. The optical paths involve linear polarized lights whose polarizations are perpendicular relative to each other, allowing the separation of the two intensity signals for modulation and detection. In case of the depolarization of the back-scattered light reflected from the diffuse object, the two intensity signals will mix in terms of their polarization states, making their complete separation impossible. Using a linearly polarized incident light, the polarization state of the back-scattered was measured, and the degree of depolarization was found to be negligible.

An intensity stabilized He-Ne laser (Newport), operating at 632.8 nm and 1.5 mW, was used as the coherent light source. The laser beam was split into two linear polarized beams with equal intensity and polarizations perpendicular relative to each other.

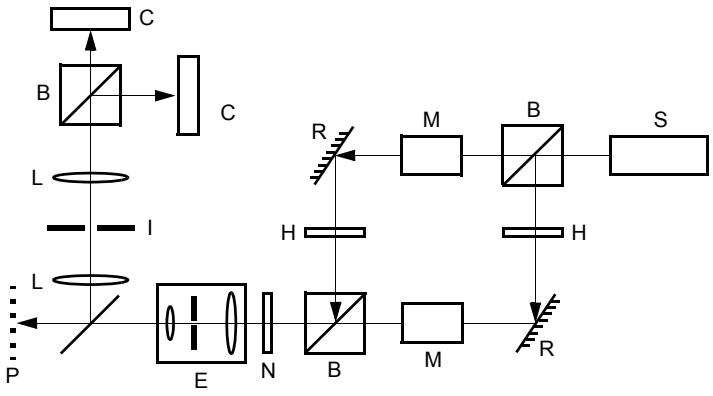


Fig. 1. Schematic diagram of the optical system. The components are labeled as: S for the laser source, B for the polarizing beam splitters, M for the modulators, R for mirrors, H for the half-wave plates, N for the neutral-density filter, E for the beam expander, P for the diffuse object, L for the lenses, I for iris, and C for the CCD sensors. The signal generator, amplifier, computer and associated electrical connections are not shown for the sake of clarity.

The intensity of the light was modulated by two Pockels cell modulators (Leysop) driven by sinusoidal voltages. The modulators were biased at 50% transmission and relatively small driving voltages were used to ensure that they responded linearly to the driving voltage. After the transmission through each modulator, the light intensity varied from 0.5 to 0.245 mW sinusoidally at the modulation frequency. Half-wave plates were used to change the *s*-polarized component to *p*-polarized component and *vice versa*, which were then recombined into a single beam by a polarizing beam splitter. The beam was expanded to a diameter of about 20 mm before arriving at the diffuse object. The subject speckle patterns were recorded by using a 4-*f* imaging system. The two polarization components were separated by a polarizing beam splitter, and each component was recorded by one of the two identical CCD sensors.

The random phase object used in the experiment was a frost glass plate with a grit number of 1500. The rough side of the plate is coated with a thin film of aluminum to make it reflecting. The plate was mounted on a translational stage (Physik Instrumente) which moved the plate surface along the in-plane direction. The light reflected by the diffuse surface was collected by a 4-*f* system consisting of two converging lenses both of which have focal lengths of 100 mm. An iris was placed in between the lenses at their common focal point. The iris opening was set at a diameter of about 2 mm, thus it acted as the aperture stop of the 4-*f* system.

Identical CCD sensors (Dalsa) were used for recording the speckle patterns. Each detector contains 1056×1056 pixels, each of which is 12 μm×12 μm in size and has a 12-bit dynamic range. The amplification setting, integration time, and triggering, *etc*., were controlled via a Labview program. The integration times ranged from 300 ms to 3 s, making them much longer than the estimated decorrelation times associated with the corresponding moving speed.

## 4. Result and discussion

A typical speckle pattern produced by a stationary random-phase object in the absence of the modulation is shown in Fig. 2**a**, which allows the autocovariance function of

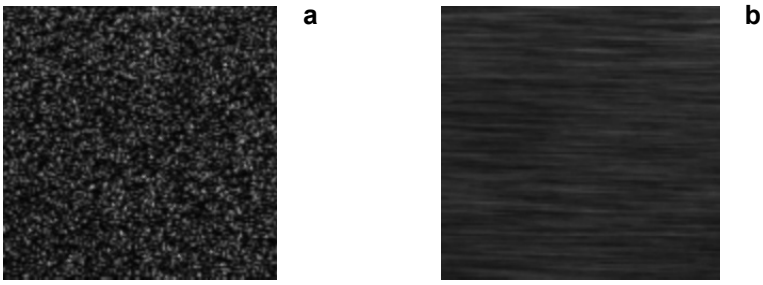


Fig. 2. A typical laser speckle pattern produced by a stationary random-phase object (**a**). A typical laser speckle pattern produced by a moving random-phase object at 1 mm/s in the absence of modulation (**b**). Both images were recorded with an integration time of 1 s, and display the same region consisting of 200×200 pixels.

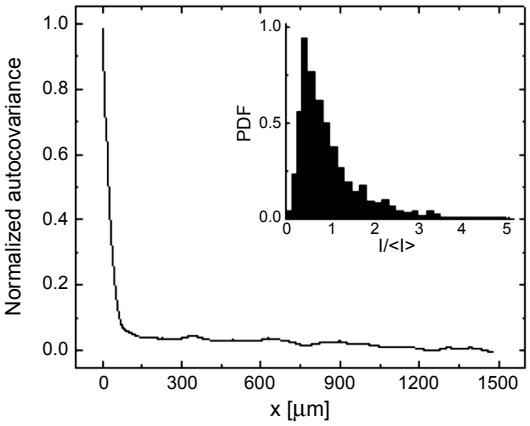


Fig. 3. The normalized autocovariance function of a stationary speckle pattern shown in Fig. 2. The inset shows the bar diagram of the probability density function (PDF) of the intensity distribution from the same stationary speckle pattern.

the intensity distribution to be determined [29]. As shown in Fig. 3, the width at half maximum of the autocovariance function along the horizontal direction was 31 μm, which was about the same for the autocovariance function along the vertical direction. The width at half maximum of the autocovariance function gives an estimate of the average speckle size [30]. Thus, the average speckle size measured in our experiment was about 2.5 times that of the CCD pixel, meeting the Nyquist criterion [31]. Note that it was also consistent with the characteristic width of the Airy function of the 4-*f* optical system used in the experiment.

The probability density function of the intensity distribution is determined from the same stationary speckle pattern. As can be seen from the inset of Fig. 3, the probability density function deviates somewhat from the ideal negative exponential curve. As the extent of depolarization was negligible, the partially developed speckle pattern is ruled out as the cause of this departure. Therefore, the main contributions were most likely the various noises presented in the experiment, such as the sensor dark current, amplifier noise, and vibration during exposure time, *etc*. [32].

Given the normal incidence and backscattering geometry used in our experiment, the dynamic speckle should be dominated by speckle translation rather than speckle boiling [33]. The speckle translation is evident in Fig. 2**b** where the speckle pattern is blurred into horizontal strips due to the in-plane motion in *x*-direction. Consequently, the time-variation of the intensity recorded at each pixel is characterized by the decorrelation time $t_c$ which depends on the speckle size and the speed of the in-plane motion. The effect of the decorrelation can be described by the normalized autocorrelation function $R(t)$ of the time-varying intensity recorded at each pixel [34]:

$$\frac{R(t)}{\bar{I}^2} = 1 + \left| 2\frac{J_1(\pi t/t_c)}{\pi t/t_c} \right|^2 \tag{7}$$

where $J_1$ is the Bessel function of the first kind, and $t_c = w/v$, with $w$ being the characteristic width of the Airy function [7] and $v$ – the speed at the image plane corresponding to the in-plane motion of the object.

Since the spatial distribution of the stationary speckle pattern can be translated into the temporal intensity fluctuation measured at a fixed pixel by simply replacing the $x$-coordinate with the elapsed time, the phase angle of the modulation is directly proportional to the $x$-coordinates of the pixels. The bright and the dark bands are formed at locations where the intensity fluctuations are in phase and out of phase with the modulation, respectively. In the speckle pattern (Fig. 4**a**) recorded by one of the cameras, the average distance between the bright and dark bands is 25 μm. For a moving speed of 1 mm/s, the corresponding time difference is 25 ms. Given a modulation frequency of 20 Hz, this time difference is the half-period of the modulation, and leads to a π phase-difference which is manifested as the alternating bright and dark bands. The speckle pattern (figure not shown) recorded simultaneously by the other camera displays similar periodicity. The intensity profiles of the speckle patterns simultaneously recorded by the two cameras are shown in Fig. 4**b**, both of which are measured along the same horizontal line of interest as marked in Fig. 4a. The periodic intensity profiles are offset horizontally by about 12 μm from each other due to the $\pi/2$ phase difference in the modulation used for each camera. When the two speckle patterns are combined by using Eq. (4), the bright-and-dark periodic structures are smoothed out, and power spectrum maps with relatively uniform intensity are obtained.

The theoretical power spectrum is readily obtained from the Fourier transform of $R(t)$ in Eq. (7), and is plotted in Fig. 5 along with the corresponding experimentally measured power spectrum. A total number of 1024 data points were used to perform

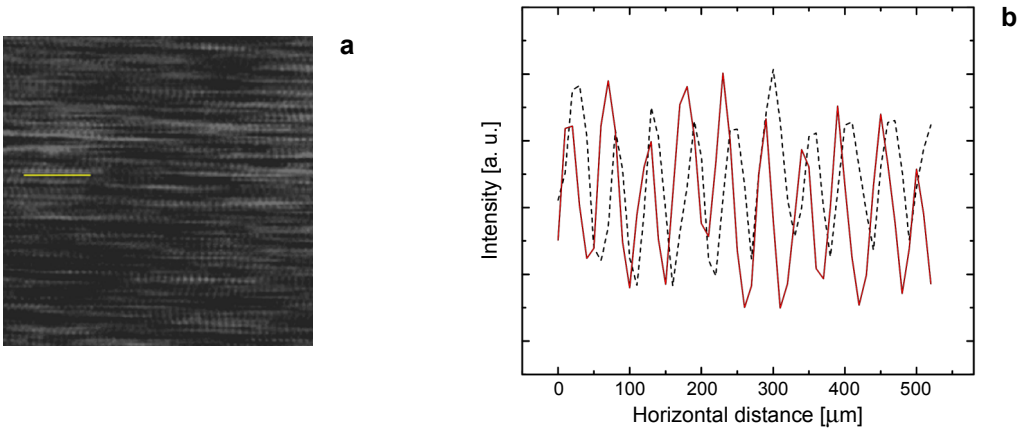


Fig. 4. A laser speckle pattern (200×200 pixels) recorded by one of the cameras, using a 20 Hz modulation and an integration time of 1 s, for a random-phase object moving at 1 mm/s (**a**). Solid line – the intensity profile measured along the horizontal line as marked in (**a**); dashed line – the intensity profile measured along the same horizontal line for the speckle pattern (figure not shown) simultaneously recorded by the other cameras; the horizontal offset between the two profiles results from the π/2 phase difference between the modulations used for recording each speckle pattern (**b**).

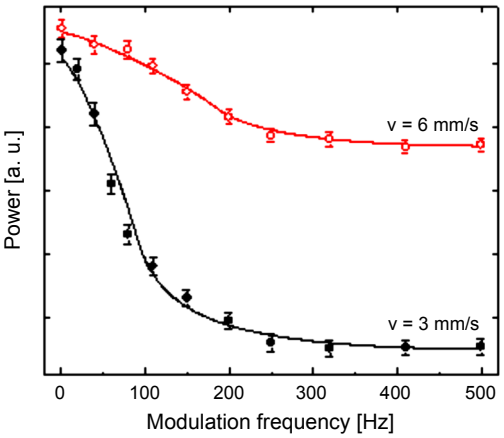


Fig. 5. The power spectra collected at two different moving speeds: 3 mm/s (solid circles) and 6 mm/s (open circles). The integration time is 1 s for both of them. The average of 225 pixels is used for each experimental data point shown. The extent of the pixel-to-pixel variation in the spectrum is shown as the error bars. The solid curves are the best fits of the experimental data points based on the model given in Eq. (7). The two spectra are offset vertically for clarity.

the Fourier transform, and the step-size of the time interval was chosen to be much smaller than the correlation time. The speed that is used to generate the theoretical power spectrum is determined by a Matlab optimization program in such a way that the optimized theoretical power spectrum gives the best fit for the corresponding experimental power spectrum. The good agreement between the two can be seen in Fig. 5. The power spectra were found to reach their peak values at 0 Hz, and their bandwidth increases consistently with increasing object moving speed, both of which are the expected results for the spectra acquired with the homodyne methods [35].

To obtain the experimental power spectrum, a ROI consisting of 15×15 pixels is chosen near the center of the speckle patterns. For each modulation frequency, the values of the power spectrum of the time-varying intensity recorded at each individual pixel are obtained. The averaged value from all 225 pixels is then used in the optimization procedure to determine the curve of the best fit. In all speckle imaging techniques, the statistical nature of the speckle pattern gives rise to the pixel-to-pixel variation [31]. The value of the power spectrum was found to vary from pixel-to-pixel, and the standard deviations resulted from this pixel-wise variation are plotted as error bars in Fig. 5.

Owning to the statistical nature of the speckle pattern and the random errors presented in the experiment, the speed values obtained via the curve fitting procedure also deviate slightly from the actual values in a random fashion. As can be seen in Fig. 6, despite of the small and random differences between the measured and the actual values of the speeds, a well-defined linear relationship can be found between the two, which illustrates the potential of this method for measuring the speed of moving diffuse objects.

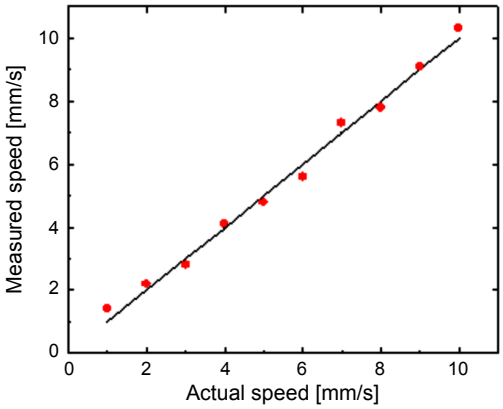


Fig. 6. The speeds obtained via the curve fitting procedure against the actual speeds used in the experiment. The solid straight line with a slope of one is shown to illustrate the linear correlation between the two.

This method relies on the use of a narrow low-pass filter which is implemented via the signal integration. To faithfully recover the power spectrum, the bandwidth of the low-pass filter (*i.e.*, the sinc function) needs to be much smaller than that of the spectrum, which translates into an integration time that is much longer than the de-correlation time. In case this requirement is not met, the operation by the low-pass filter, as given in Eq. (6), will lead to the overestimation of the lower frequency spectral components and the appearance of oscillatory features in the spectrum.

The effect of the small integration time is illustrated in Fig. 7, where two power spectra are shown, both of which were obtained for a moving speed of 6 mm/s.

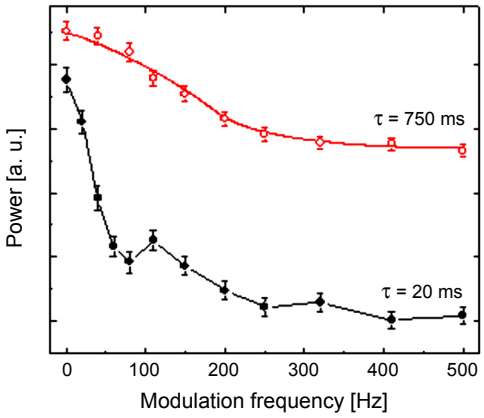


Fig. 7. Power spectra measured using two different integration times: 20 ms (solid circles) and 750 ms (open circles). The moving speed is 6 mm/s for both of them. The straight lines connecting the solid circles are guides for the eyes. The solid curve next to the open circles is the best fit of the experimental data points based on the model given in Eq. (7). The average of 225 pixels is used for each data point shown. The extent of the pixel-to-pixel variation in the spectrum is shown as the error bar. The two spectra are offset vertically for clarity.

However, one was obtained with an integration time of 750 ms; while the other one with 20 ms. Because the decorrelation time is 5.2 ms, the latter integration time is not adequate, and the substantially modification of the power spectrum can be observed in Fig. 7.

## 5. Conclusions

In conclusion, we have demonstrated an approach for analyzing the power spectrum of the time-varying intensity presented in dynamic laser speckle patterns. The use of the temporal-intensity-modulation and the subsequent low-pass filtering allow the value of the power spectrum at the modulation frequency to be extracted. By taking advantage of the charge accumulation nature of the CCD sensors for the purpose of the signal integration, the data acquisition and processing procedures are greatly simplified. The method is free from the limitation imposed by the Nyquist criterion on the minimum sampling rate, allowing it to be implemented using multiple-channel detectors with limited frame rates for the application of full-field imaging of speed and flow distributions.

To determine the power spectrum over a frequency range, the modulation frequency will need to be scanned over that range. It was found, however, that the curve fitting procedure can be performed with good confidence by using as few as ~10 data points for the experimental power spectrum. The absence of complex and sharp features in the power spectra observed in our experiment justifies the use of fewer numbers of data points. Within the speed range from 1 to 10 mm/s investigated in our experiment, the result demonstrates that the moving speed of the diffuse object can be determined with a good accuracy provided that the integration time is much longer than the decorrelation time. The substantial modifications in the power spectra were observed when the requirement on the integration time was not met.

Future study of the full-field temporal modulation method will utilize live tissue samples where the dynamic laser speckle pattern is generated by the blood flow and perfusion in vascular systems. The power spectra obtained with this method will allow the extraction of dynamic signals associated with blood flow and perfusion, and the rejection of the static noise generated due to the scattering of connective tissues. Therefore, this method will greatly improve the signal-to-noise ratio of the recorded flow pattern, allowing microcirculations in small vessels to be investigated.

*Acknowledgements* – The authors would like to acknowledge the support of NSF RII South Carolina EPSCoR program on tissue engineering.

### References

[1] BRIERS J.D., *Laser Doppler, speckle and related techniques for blood perfusion mapping and imaging*, Physiological Measurement **22**(4), 2001, pp. R35–R66.

[2] PENGCHENG LI, SONGLIN NI, LI ZHANG, SHAOQUN ZENG, QINGMING LUO, *Imaging cerebral blood flow through the intact rat skull with temporal laser speckle imaging*, Optics Letters **31**(12), 2006, pp. 1824–1826.

[3] WEBER B., BURGER C., WYSS M.T., VON SCHULTHESS G.K., SCHEFFOLD F., BUCK A., *Optical imaging of the spatiotemporal dynamics of cerebral blood flow and oxidative metabolism in the rat barrel cortex*, European Journal of Neuroscience **20**(10), 2004, pp. 2664–2670.

[4] DURDURAN T., BURNETT M.G., GUOQIANG YU, CHAO ZHOU, DAISUKE FURUYA, YODH A.G., DETRE J.A., GREENBERG J.H., *Spatiotemporal quantification of cerebral blood flow during functional activation in rat somatosensory cortex using laser-speckle flowmetry*, Journal of Cerebral Blood Flow and Metabolism **24**(5), 2004, pp. 518–525.

[5] DUNN A.K., DEVOR A., BOLAY H., ANDERMANN M.L., MOSKOWITZ M.A., DALE A.M., BOAS D.A., *Simultaneous imaging of total cerebral hemoglobin concentration, oxygenation, and blood flow during functional activation*, Optics Letters **28**(1), 2003, pp. 28–30.

[6] VÖLKER A.C., ZAKHAROV P., WEBER B., BUCK F., SCHEFFOLD F., *Laser speckle imaging with an active noise reduction scheme*, Optics Express **13**(24), 2005, pp. 9782–9787.

[7] ZAKHAROV P., VÖLKER A.C., BUCK A., WEBER B., SCHEFFOLD F., *Quantitative modeling of laser speckle imaging*, Optics Letters **31**(23), 2006, pp. 3465–3467.

[8] DUNCAN D.D., KIRKPATRICK S.J., *Can laser speckle flowmetry be made a quantitative tool?*, Journal of the Optical Society of America A **25**(8), 2008, pp. 2088–2094.

[9] RAJAN V., VARGHESE B., VAN LEEUWEN T.G., STEENBERGEN W., *Review of methodological developments in laser Doppler flowmetry*, Lasers in Medical Science **24**(2), 2009, pp. 269–283.

[10] LINDÉN M., *Can blood flow in separate small tubes be quantitatively assessed by high-resolution laser Doppler imaging?*, Medical and Biological Engineering and Computing **35**(6), 1997, pp. 575–580.

[11] HUMEAU A., SAUMET J.L., L'HUILLIER J.P., *Laser Doppler blood flowmetry multiple scattering study during reactive hyperaemia*, Proceedings of SPIE **4163**, 2000, pp. 9–17.

[12] JENTINK H.W., DE MUL F.F.M., HERMSEN R.G.A.M., GRAAFF R., GREVE J., *Monte Carlo simulations of laser Doppler blood flow measurements in tissue*, Applied Optics **29**(16), 1990, pp. 2371–2381.

[13] FEKE G.T., RIVAT C.E., *Laser Doppler measurements of blood velocity in human retinal vessels*, Journal of the Optical Society of America **68**(4), 1978, pp. 526–531.

[14] DÖRSCHEL K., MÜLLER G., *Velocity resolved laser Doppler blood flow measurements in skin*, Flow Measurement and Instrumentation **7**(3–4), 1996, pp. 257–264.

[15] IMAI Y., TANAKA K., *Direct velocity sensing of flow distribution based on low-coherence interferometry*, Journal of the Optical Society of America A **16**(8), 1999, pp. 2007–2012.

[16] BONNER R., NOSSAL R., *Model for laser Doppler measurements of blood flow in tissue*, Applied Optics **20**(12), 1981, pp. 2097–2107.

[17] FITZAL F., VALENTINI D., WORSEG A., HOLLE J., REDI H., *Evaluation of total vs. regional blood perfusion with a laser Doppler imaging system in the rat epigastric flap*, Journal of Reconstructive Microsurgery **17**(1), 2001, pp. 59–67.

[18] ABBISS J.B., CHUBB T.W., PIKE E.R., *Laser Doppler anemometry*, Optics and Laser Technology **6**(6), 1974, pp. 249–261.

[19] ESSEX T.J.H., BYRNE P.O., *A laser Doppler scanner for imaging blood flow in skin*, Journal of Biomedical Engineering **13**(3), 1991, pp. 189–194.

[20] FERRELL W.R., BALINT P.V., STURROCK R.D., *Novel use of laser Doppler imaging for investigating epicondylitis*, Rheumatology **39**(11), 2000, pp. 1214–1217.

[21] CHOWDHURY D.P., SORENSEN C.M., TAYLOR T.W., MERKLIN J.F., LESTER T.W., *Application of photon correlation spectroscopy to flowing Brownian motion systems*, Applied Optics **23**(22), 1984, pp. 4149–4154.

[22] WEBER R., SCHWEIGER G., *Photon correlation spectroscopy on flowing polydisperse fluid-particle systems: theory*, Applied Optics **37**(18), 1998, pp. 4039–4050.

[23] MEYER W.V., SMART A.E., BROWN R.G.W., ANISIMOV M.A., *Photon correlation and scattering: introduction to the feature issue*, Applied Opticss **36**(30), 1997, pp. 7477–7479.

[24] NARAYANAN T., CHEUNG C., TONG P., GOLDBURG W.I., WU X.L., *Measurement of the velocity difference by photon correlation spectroscopy: an improved scheme*, Applied Optics **36**(30), 1997, pp. 7639–7644.

[25] DRAIJER M., HONDEBRINK E., VAN LEEUWEN T.G., STEENBERGEN W., *Twente Optical Perfusion Camera: system overview and performance for video rate laser Doppler perfusion imaging*, Optics Express **17**(5), 2009, pp. 3211–3225.
[26] JOON HYUK PARK, PLATISA J., VERHAGEN J.V., GAUTAM S.H., OSMAN A., DONGSOO KIM, PIERIBONE V.A., CULURCIELLO E., *Head-mountable high speed camera for optical neural recording*, Journal of Neuroscience Methods **201**(2), 2011, pp. 290–295.
[27] MEYERS J.F., *Development of Doppler global velocimetry as a flow diagnostics tool*, Measurement Science and Technology **6**(6), 1995, pp. 769–783.
[28] FUJII H., NOHIRA K., YAMAMOTO Y., IKAWA H., OHURA T., *Evaluation of blood flow by laser speckle image sensing. Part 1*, Applied Optics **26**(24), 1987, pp. 5321–5325.
[29] GOODMAN J.W., *Statistical properties of laser speckle pattern*, [In] *Laser Speckle and Related Phenomena*, [Ed.] J.C. Dainty, Vol. 9, Springer-Verlag, Berlin, Heidelberg, New York, Tokyo, 1984.
[30] CARVALHO O., CLAIRAC B., BENDERITTER M., ROY L., *Statistical speckle study to characterize scattering media: use of two complementary approaches*, Optics Express **15**(21), 2007, pp. 13817–13831.
[31] DUNCAN D.D., KIRKPATRICK S.J., WANG R.K., *Statistics of local speckle contrast*, Journal of the Optical Society of America A **25**(1), 2008, pp. 9–15.
[32] ALEXANDER T.L., HARVEY J.E., WEEKS A.R., *Average speckle size as a function of intensity threshold level: comparison of experimental measurements with theory*, Applied Optics **33**(35), 1994, pp. 8240–8250.
[33] YOSHIMURA T., NAKAGAWA K., WAKABAYASHI N., *Rotational and boiling motion of speckles in a two-lens imaging system*, Journal of the Optical Society of America A **3**(7), 1986, pp. 1018–1022.
[34] GOODMAN J.W., *Speckle Phenomena in Optics: Theory and Applications*, Roberts and Company Publishers, 2007, pp.78–80.
[35] BRIERS J.D., *Laser Doppler and time-varying speckle: a reconciliation*, Journal of the Optical Society of America A **13**(2), 1996, pp. 345–350.

*Received August 31, 2012*
*in revised form February 18, 2013*